Rationale: Characterization of Regolith And Trace Economic Resources (CRATER), an

Article *in* Rapid Communications in Mass Spectrometry · February 2024

DOI: 10.1002/rcm.9657

20 authors, including:

Soumya Ray
University of Maryland, College Park
9 PUBLICATIONS **38** CITATIONS
SEE PROFILE

Ricardo Arevalo Jr.
University of Maryland, College Park
66 PUBLICATIONS **1,803** CITATIONS
SEE PROFILE

Adrian E. Southard
Universities Space Research Association
37 PUBLICATIONS **379** CITATIONS
SEE PROFILE

Lori Willhite
University of Maryland, College Park
12 PUBLICATIONS **99** CITATIONS
SEE PROFILE

Received: 27 June 2023 | Revised: 29 September 2023 | Accepted: 1 October 2023

DOI: 10.1002/rcm.9657

RESEARCH ARTICLE

Rapid Communications in Mass Spectrometry WILEY

Characterization of Regolith And Trace Economic Resources (CRATER): An Orbitrap-based laser desorption mass spectrometry instrument for in situ exploration of the Moon

Soumya Ray[1] | Ricardo Arévalo Jr[1] | Adrian Southard[2] | Lori Willhite[1] | Anais Bardyn[1] | Ziqin Ni[1] | Ryan Danell[3] | Andrej Grubisic[4] | Cynthia Gundersen[5] | Julie Llano[5] | Anthony Yu[4] | Molly Fahey[4] | Emanuel Hernandez[4] | Jacob Graham[4] | Jane Lee[4] | Akif Ersahin[6] | Christelle Briois[7] | Laurent Thirkell[7] | Fabrice Colin[7] | Alexander Makarov[8]

[1]University of Maryland, College Park, Maryland, USA

[2]CRESST II, College Park, Maryland, USA

[3]Danell Consulting, Winterville, North Carolina, USA

[4]NASA Goddard Space Flight Center, Greenbelt, Maryland, USA

[5]AMU Engineering, Miami, Florida, USA

[6]MAE Aerospace, South Glastonbury, Connecticut, USA

[7]Laboratoire de Physique et Chimie de l'Environnement et de l'Espace, Orléans, France

[8]Thermo Fisher Scientific, Bremen, Germany

Correspondence
Soumya Ray, University of Maryland, College Park, MD, USA.
Email: soumray@umd.edu

Funding information
The work presented here was supported by the NASA ROSES DALI Grant 80NSSC19K0768 (PI: R.A. Jr), NASA ROSES ICEE 2 Grant 80NSSC19K0610 (PI: R.A. Jr), University of Maryland Faculty Incentive Program (PI: R.A. Jr), NASA Goddard Space Flight Center Internal Research and Development Program (PIs: A.G. and A.Y.), CRESST II Award Number 80GSFC21M0002 (PI: A.S.), and CNES for CosmOrbitrap development.

Rationale: Characterization of Regolith And Trace Economic Resources (CRATER), an Orbitrap™-based laser desorption mass spectrometry instrument designed to conduct high-precision, spatially resolved analyses of planetary materials, is capable of answering outstanding science questions about the Moon's formation and the subsequent processes that have modified its (sub)surface.

Methods: Here, we describe the baseline design of the CRATER flight model, which requires <20 000 cm^3 volume, <10 kg mass, and <60 W peak power. The analytical capabilities and performance metrics of a prototype that meets the full functionality of the flight model are demonstrated.

Results: The instrument comprises a high-power, solid-state, pulsed ultraviolet (213 nm) laser source to ablate the surface of the lunar sample, a custom ion optical interface to accelerate and collimate the ions produced at the ablation site, and an Orbitrap mass analyzer capable of discriminating competing isobars via ultrahigh mass resolution and high mass accuracy. The CRATER instrument can measure elemental and isotopic abundances and characterize the organic content of lunar surface samples, as well as identify economically valuable resources for future exploration.

Conclusion: An engineering test unit of the flight model is currently in development to serve as a pathfinder for near-term mission opportunities.

1 | INTRODUCTION

The Artemis program will herald a new age of scientific discovery and exploration centered around the Moon. To this end, the development of payloads that support scientific understanding, technological advancements, in situ resource utilization, and human exploration objectives is a critical need. Specifically, instruments that can leverage progressive technologies provided by NASA's Commercial Lunar Payload Services (CLPS) initiative will help strengthen the foundation on which future missions to and from the Moon will rely.

Our understanding of the formation and evolution of the Moon has evolved due to remote sensing instruments that have provided near-global coverage of the chemical and mineralogical composition of the lunar surface, albeit with limited spatial resolution.[1–6] Laboratory-based analyses of lunar meteorites[7,8] and lunar samples brought back by the Apollo,[9,10] Luna,[11] and Chang-e[12,13] missions have also provided unprecedented insights into the compositional makeup of the lunar (sub)surface. However, geological context for lunar meteorites is often lacking, and sample return missions are resource intensive and have low cadence. Thus, to complement the insights gleaned from remote sensing orbiters and laboratory analyses of returned samples and meteorites, spaceflight instruments that are able to conduct chemical analyses in situ at high spatial resolution need to be innovated to maximize this new era of lunar exploration.

Applications of laser desorption mass spectrometry (LDMS) have been demonstrated as far back as the 1960s[14]; such techniques, which are common in the commercial realm, are beginning to find a niche in planetary exploration.[15–20] Laser-enabled in situ methods enable spatially resolved analyses, minimize analytical blanks, and limit risks of contamination by avoiding direct contact with the sample. Compared to longer wavelengths, ultraviolet (UV) light is efficiently absorbed by a variety of geologically relevant minerals and glasses[21] as well as a wide range of refractory organic compounds,[22] leading to efficient ablation/desorption. Therefore, UV laser sources offer access to a spectrum of samples of geological and astrobiological significance. Once the analyte has been desorbed and ionized, a mass analyzer with the capability of resolving analyte ions with nominally overlapping or similar mass-to-charge ratios (m/z) is critical for detection and accurate identification of elemental and molecular

TABLE 1 CRATER flight model characteristics.

Parameter	Value
Laser output wavelength	213 nm
Maximum output energy	1 mJ (at 213 nm)
Variable attenuation	0–100% in 5% steps
Laser spot size	50 μm diameter
Laser fluence	2–30 J cm^{-2} (45° incidence)
Total mass	<10 kg
Total volume	<20 000 cm^3
Peak power	<60 W
Operation limit[a]	−20 to +50°C
Survival limit[b]	−30 to +60°C
Mass range	20–2000 u
Mass resolving power[c]	~120 000 at m/z ^{133}Cs
Mass accuracy[c]	± 6 ppm

[a]Upper limit for operation of Orbitrap mass analyzer (+75°C) and laser head (+50°C).
[b]Upper limit for survival of Orbitrap mass analyzer (+115°C) and laser head (+60°C).
[c]As demonstrated by analyses conducted on the CRATER prototype in this study.

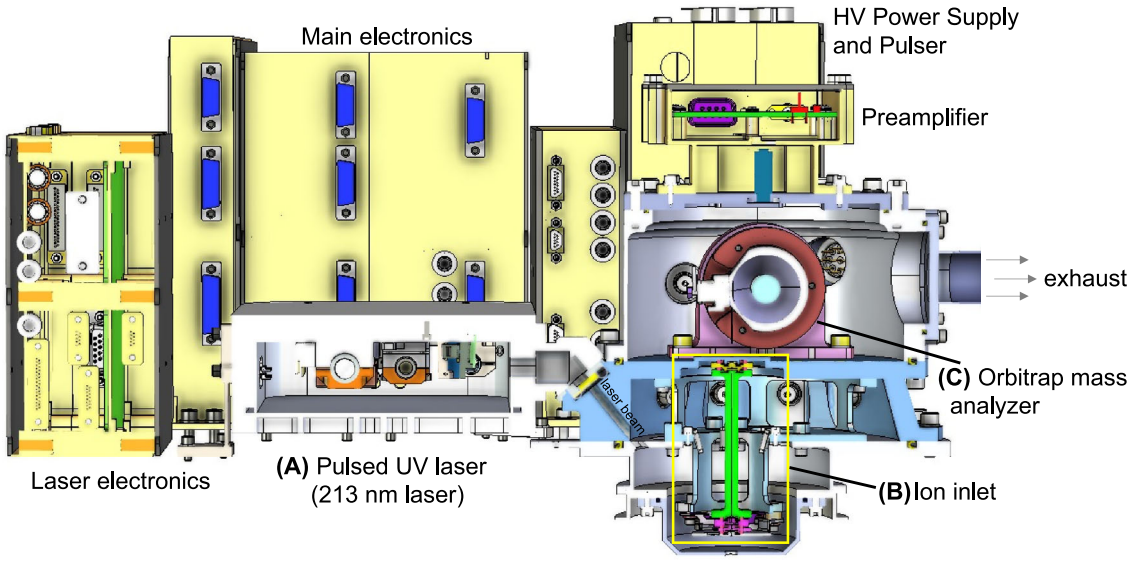

FIGURE 1 Cross-section of a solid model of the CRATER flight instrument, which integrates (A) a high-power UV laser source (Section 2.1), (B) a custom series of ion optics (Section 2.2 and Figure 3), and (C) an Orbitrap mass analyzer (Section 2.3). Also shown is the preamplifier, which amplifies and digitizes ion signal. The laser electronics, main electronics, and high-voltage power supply that support the operation of CRATER are also shown (Section 2.5). The flight design requires <20,000 cm^3 volume (including electronics boxes), <10 kg total mass, and <60 W peak power. [Color figure can be viewed at wileyonlinelibrary.com]

species. Thus far, spaceflight mass spectrometers designed to analyze nonvolatile targets have incorporated time-of-flight mass analyzers (e.g., the Cometary Secondary Ion Mass Analyzer, COSIMA[23]) or linear ion traps (e.g., the Mars Organic Molecular Analyzer, MOMA[16]) that offer limited mass resolving powers (<1400, full width half maximum [FWHM] at *m/z* 100). The Orbitrap mass analyzer, originally developed for the commercial industry,[24] is now being adapted for spaceflight mass spectrometry due to its ultrahigh mass resolving power (>100,000 FWHM at *m/z* 100) and mass accuracy (ppm level).[18,20,25–29]

The Characterization of Regolith And Trace Economic Resources (CRATER) instrument, an Orbitrap-based LDMS instrument specifically designed for operations on the Moon's surface, is capable of collecting two-dimensional (2D) chemical maps and 3D depth profiles of sample mineralogy/elemental chemistry and organic diversity in lunar surface materials. Here we describe the design and characteristics of the CRATER flight model (Figure 1 and Table 1), demonstrate the performance of a prototype instrument that meets the full functionality of the flight design, and discuss general operations of the CRATER instrument during a prospective lunar mission.

2 | CRATER FLIGHT MODEL DESIGN

2.1 | Pulsed UV (213 nm) laser subsystem

Similar to the Mercury Laser Altimeter (MLA) flown on the MESSENGER mission,[30] the CRATER laser centers on a master oscillator power amplifier that uses Cr:Nd:YAG as the gain medium, producing a fundamental wavelength of 1064 nm. The oscillator (Figure 2A) consists of a crossed-Porro optical resonator with polarization output coupling, Cr:Nd:YAG gain slab, two polarizing beam splitter cubes, passive Q-switch, multiple zero-order quartz wave plates for polarization control, and fused-silica Risley wedges for optical adjustment/alignment. The oscillator output undergoes a beam expansion (2× magnification), then is injected into the power amplifier through the second beam splitter. The light passes through the Cr:Nd:YAG power amplifier slab twice for an overall gain of 8.7 dB,[30] ultimately resulting in the emission of ~20 mJ at the fundamental wavelength.

The CRATER laser is designed to operate at the fifth harmonic (213 nm, 5.8 eV/photon) to promote photon-substrate coupling and enhance laser ablation efficiency.[31] To accomplish this, the fundamental beam is routed via a periscope through a series of harmonic generators (i.e., nonlinear frequency conversion crystals) located on the opposite side of the laser bench (Figure 2B). Second-harmonic generation produces 532 nm light, which is mixed with residual 1064 nm to generate 355 nm in the third harmonic. Finally, the 355 nm light and residual 532 nm are mixed to generate 213 nm radiation. The maximum expected UV pulse energy (>1 mJ at 213 nm) equates to an overall conversion efficiency of ~5%. Laser output energies can be tuned between 0% and 100% of maximum in increments of 5% by way of a Pockels cell in the laser transmitter; tunable laser energy (and by extension fluence, or energy density in J/cm^2) enables efficient desorption/ablation of a sample depending on its intrinsic ablation threshold. The CRATER laser has selectable repetition rates between 1 and 10 Hz and a pulse width of 5 ns. Supported by a micro electro-mechanical systems (MEMS) steering mirror, the laser beam can be scanned across the surface of the sample with an effective field of view of 500 µm (diameter), enabling 2D chemical mapping without manipulation of the sample.[32] The CRATER laser gain medium is doped with Cr^{3+} (i.e., Cr:Nd:YAG) to prevent radiation-induced darkening that may lead to degraded performance through the mission life.

The laser electronics terminate the laser diode driver once a Q-switched laser pulse is generated to avoid overheating of the gain medium. A photodiode located behind the periscope on the oscillator side of the laser bench is employed to detect the laser pulse and initiate the LDMS experimental sequence. A second photodiode located after the 213 nm beam expander is used to monitor the output energy. The mechanical design of the laser housing utilizes a

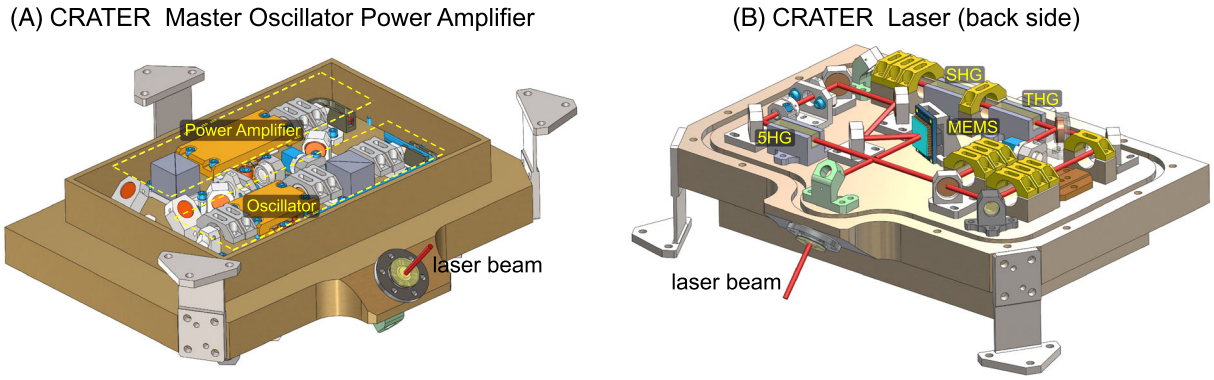

FIGURE 2 (A) Schematic diagram of the CRATER master oscillator power amplifier that leverages the heritage design of the Mercury Laser Altimeter flown on the MESSENGER mission. (B) Harmonic generators housed on the opposite side of the laser bench transform the fundamental wavelength (1064 nm) to the CRATER output UV wavelength (213 nm). The micro-electro-mechanical systems (MEMS) steering mirror enables 2D chemical mapping by scanning the sample surface without requiring translation or rotation of the sample. The red line illustrates the path of the laser beam through the various harmonic generators (B) and the final emergence of the 213 nm UV laser beam. SHG, second-harmonic generator; THG, third-harmonic generator; 5HG, fifth-harmonic generator. [Color figure can be viewed at wileyonlinelibrary.com]

beryllium optical bench to reduce mass and enhance thermal performance. A Ti_6Al_4V spacer ensures maximum thermal isolation of the bench from the rest of the CRATER instrument. A thermoelectric cooler is used to regulate the temperature of the oscillator, which is heat sunk to a thermally isolated bench to keep the laser diode array at its design temperature (+50°C to support daytime lunar operations) and aligned to the absorption peak of the gain medium.

2.2 | Ion inlet subsystem

The CRATER ion inlet consists of a series of electrostatic and electroactive lenses (Figure 3) that ultimately direct ions generated by irradiation of the sample towards the Orbitrap mass analyzer (Section 2.3). At a working distance between 5 and 10 mm (set at 6 mm in the baseline design) from the sample surface is the extractor lens that uses high voltage (typically ±3000 V) to accelerate ions further into the inlet. The ions are subsequently decelerated by focus lens 1 at an intermediate voltage before they encounter two pairs of deflector electrodes that serve to (i) further decelerate the ions and (ii) steer the ions toward the center of the elevator electrode during active laser scanning across the sample surface. The voltage and operation of the elevator electrode is contingent on the presentation of the lunar sample and mode of deployment of CRATER on the lunar surface (see Section 3 and Table 2 for details). If the sample is actively floated to a nonzero voltage, the elevator electrode can be grounded and act as a de facto drift tube.[18] However, if the sample is held at ground potential (0 V), the elevator electrode needs to be pulsed to provide an energy "lift" to the ions to achieve stable trajectories.[33] Focus lens 2 provides ultimate focusing of the ions before injection into the Orbitrap mass analyzer.

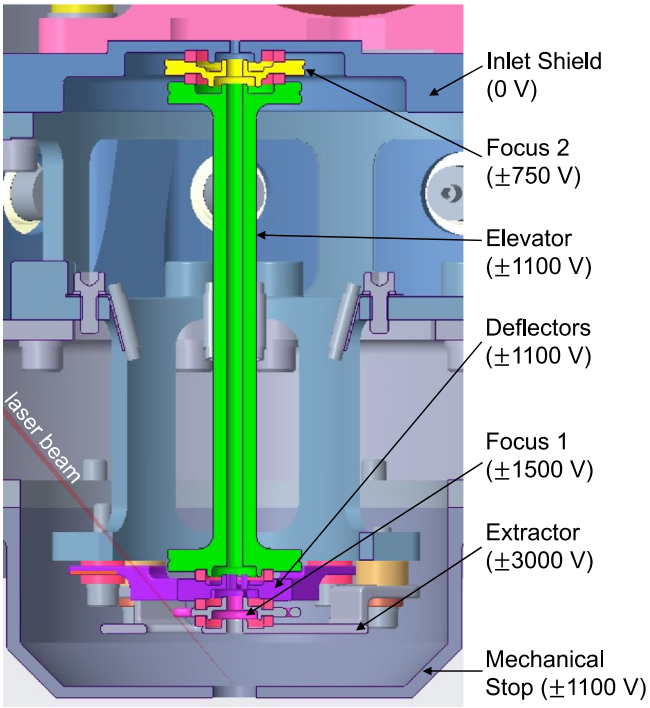

FIGURE 3 Cut-away view of a solid model of the ion inlet enclosed within the mechanical stop assembly. The laser beam has an angle of incidence of 45° to the sample plane. Ions generated at the surface of the sample are guided and collimated by a series of ion optical lenses. The ion inlet subsystem supports operations in dual polarity, as reflected by notional voltage ranges. Thus, CRATER is capable of detecting both positive ions (i.e., cations) and negative ions (i.e., anions). [Color figure can be viewed at wileyonlinelibrary.com]

2.3 | Orbitrap mass analyzer

Once the ions are collimated by the ion inlet, they are injected into the Orbitrap mass analyzer, which consists of four discrete electrodes: two axially symmetric outer electrodes, the central electrode (CE), and the deflector electrode (DE) that compensates for fringe fields caused by the aperture through which ions enter the analyzer. The geometry of the electrodes produces quadro-logarithmic electrostatic potentials that enable "orbital trapping" of ions[24]; no magnets or radio frequency fields are required. During ion injection, the outer electrodes are grounded while the voltages applied to the CE and DE are ramped, typically over 20–100 μs.[33,34] This leads to intensification of the electric fields experienced by the ions such that they are "electrodynamically squeezed" toward the CE. Thereafter, the successfully trapped ions oscillate harmonically about the CE at axial frequencies inversely proportional to the square root of their respective mass-to-charge ratio (m/z).

The axial frequencies of the trapped ions are detected as image current, which is amplified and digitized by a preamplifier at a sampling rate at or above the Nyquist frequency of the highest frequency analyte ion to accurately record the transient signal. This transient is transmuted into a frequency spectrum via fast Fourier transform (FFT). The frequency domain signal can be converted into a mass spectrum through the relationship: $\omega = \sqrt{(kq/m)}$, where ω is the axial frequency, k is the axial restoring force, q is the charge of the ion, and m is the ion mass. The Orbitrap mass analyzer adapted for spaceflight offers ultrahigh mass resolving powers up to $m/\Delta m$ > 100,000 (FWHM at m/z 100) and parts per million (ppm)-level mass accuracy, enabling the unambiguous detection and identification of molecular, elemental, and isotopic signals.[18,20,25–29]

2.4 | Mechanical design

The driving requirement for the mechanical design of the CRATER flight model is to limit interface responses such as displacement, shear stress, etc. to ensure survival when subjected to general environmental verification specification (GEVS) qualification-level random vibration (i.e., 14.1 grms) and thermal qualification (i.e., −30°C up to +115°C to support dry heat microbial reduction). To facilitate machinability, assembly, and integration, the hermetically sealed analyzer housing is split into two distinct volumes: the lower and upper housing chambers. The Orbitrap mass analyzer, supported by two brackets to reduce the

TABLE 2 Ion inlet parameters used in the SIMION ion and optics simulator to constrain focus 1 and 2 (F1 and F2) voltages that enable high ion transmission as a function of target/sample voltage and sample height with respect to the mechanical stop (i.e., *y* offset). Also shown is how each of the examples of sample characteristics potentially corresponds to mode of sample delivery to CRATER on the Moon.

	Parameters	Sample at voltage, no *y* offset (Figure 6A)	Sample at voltage, *y* offset (Figure 6B)	Sample grounded, no *y* offset (Figure 6C)	Sample grounded, *y* offset (Figure 6D)
Input	Mechanical stop voltage	+1100 V	+1100 V	0 V	0 V
	Extractor lens voltage	−1900 V	−1900 V	−2900 V	−2900 V
	Elevator electrode voltage	0 V	0 V	Pulsed from −1100 to 0 V	Pulsed from −1100 to 0 V
	Potential sag compensation	Not required	Applied by increasing voltage on target to +1460 V	Not required	Applied by pulsing elevator electrode and deflectors from −1420 to 0 V
Output	Recommended F1 voltage	−1800 to +200 V	−2200 to −1600 V or 0 to +300 V	−2900 to −1000 V	−3700 to −3200 V or −1300 to −1100 V
	Recommended F2 voltage	+200 to +400 V or −500 to −750 V	+250 to +400 V or −600 to −800 V	+200 to +400 V or −500 to −750 V	+250 to +400 V or −600 to −800 V
Increasing requirements	**Corresponding modes of sample analyses**				
	CRATER lowered to the lunar surface via tether or mechanism		✓	✓	✓
	Regolith sampled and flattened by a robotic arm	✓		✓	
	Regolith sampled by robotic arm with no flattening		✓		✓

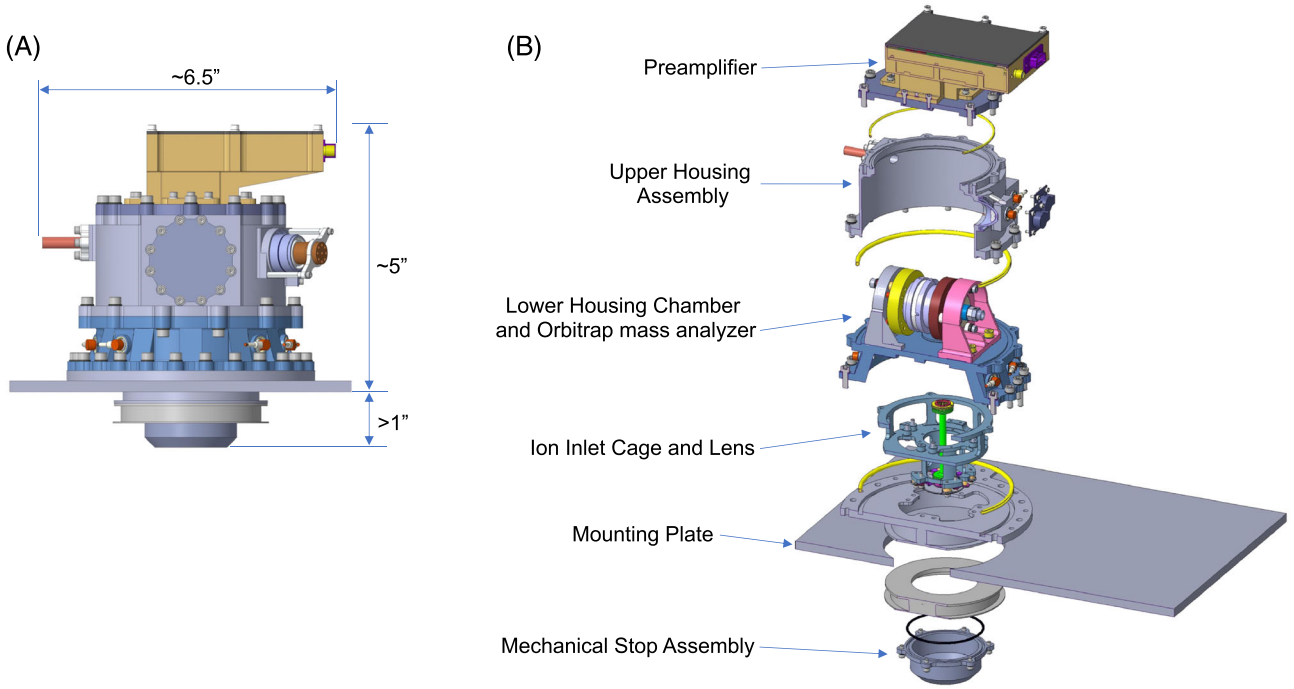

FIGURE 4 (A) Mechanical design of the CRATER instrument. The CRATER instrument's stiff and compact design is optimized to survive project launch loads for a variety of missions while its low mass (<10 kg) makes it amenable to a wide range of landers, rovers, and mission weight caps. (B) An exploded-view of the CRATER instrument illustrating its various components. [Color figure can be viewed at wileyonlinelibrary.com]

propagation of launch loads, sits on the plate that separates these chambers (Figure 4). In addition to providing structural support to the Orbitrap mass analyzer, the lower housing chamber incorporates the final aperture of the ion inlet subsystem (immediately following focus lens 2), designated as the reference point for the entire ion inlet. The aperture guides the alignment between the lens stack and the entrance to the Orbitrap analyzer during assembly. The ion inlet has strict requirements that the lenses be aligned within 20 μm of the reference point while maintaining parallelism within ±127 μm, with respect to the sample plane. The allowable margins, as empirically measured between the theoretical axis and the lens inner diameters, are allocated to ensure ions follow optimal trajectories into the Orbitrap mass analyzer. Additionally, the lower housing chamber comprises a brazed laser window to allow the laser beam to reach the sample while maintaining the hermeticity of the chamber; welded feedthroughs serve as hermetic pathways for providing voltages to the lenses.

The upper housing chamber encloses and protects the Orbitrap mass analyzer, supports the hard-mounted preamplifier electronics board, and safely delivers high voltages to the deflector and central electrodes through welded hermetic feedthroughs. Both lower and upper chambers have been designed to minimize mass and reduce machining complexity (cost) while also supporting ultrahigh vacuum using gold-plated Inconel C-seals (versus elastomer O-rings with high permeabilities) and high strength hardware (i.e., stainless steel alloy, A286) throughout. The CRATER mounting plate and mechanical stop assembly provide an alignment reference for the laser. In addition, the mechanical stop facilitates sample introduction and is critical to maintain sample height from a nominal reference plane (*y* offset) that dictates the operation voltages for efficient ion transmission (Section 3).

2.5 | Electrical architecture and control

The CRATER electrical architecture is based around several electrical components that serve specific purposes to enable the complete Orbitrap-based LDMS experiment (Figure 1). The main electronics box includes standard power supplies for interfacing with the spacecraft power bus(es). There is a separate laser electronics board for controlling and monitoring the laser subsystem, as well as high voltage power supplies to generate the necessary voltages for the ion inlet system and the Orbitrap analyzer electrodes. The design also includes two different pulsed voltage supplies to provide necessary time varying voltage levels to the elevator electrode in the ion inlet and the CE and DE within the Orbitrap analyzer. The transient signal generated from the induced current on the outer electrodes of the Orbitrap analyzer is amplified by a preamplifier mounted on the vacuum housing for minimal signal loss and to reduce noise introduction. Finally, the control and monitoring of the entire instrument, and specifically the Orbitrap-based LDMS experiment, is accomplished through a communication, control and data handling board within the main electronics. The control board handles health

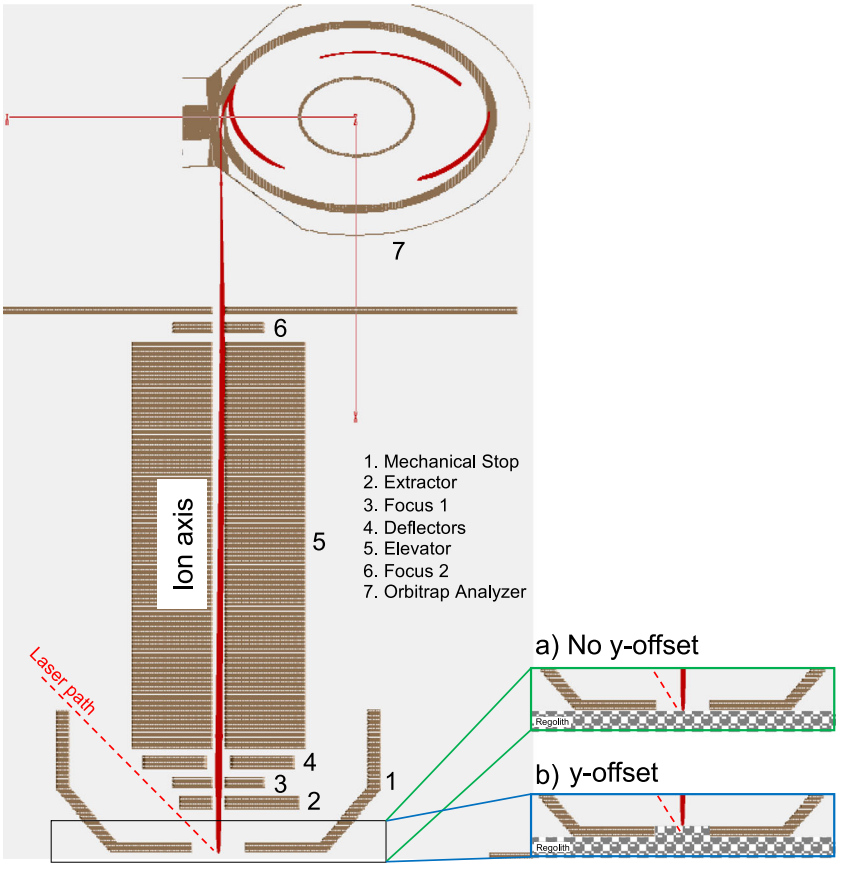

FIGURE 5 Schematic of the SIMION® ion and electron optics simulator illustrating the mechanical stop, ion inlet, and Orbitrap mass analyzer. (A) "No *y* offset" represents the case scenario when the boundary of the regolith/dielectric medium is level with the bottom of the mechanical stop such that there is no sample protrusion and (B) "*y* offset" illustrates the case when the regolith boundary protrudes into the mechanical stop, which then necessitates application of the potential sag compensation to ensure high ion transmission. [Color figure can be viewed at wileyonlinelibrary.com]

and safety monitoring of the instrument, the key laser and experiment timing and synchronization tasks for the Orbitrap mass analyzer, transient signal data collection, and FFT data processing to allow conversion of the acquired data into a mass spectrum onboard the instrument hardware.

3 | ION TRANSMISSION SIMULATIONS FOR CRATER

To constrain voltages for operation of the CRATER instrument, we simulated the transmission of ions generated at the surface of the sample target, collimated through the ion inlet, and injected into stable orbits within the Orbitrap mass analyzer. Ion transmission is denoted as *T* % and defined as the percentage of ions generated from the target that acquire stable trajectories around the central electrode (and thereby avoid collision with the outer electrodes of the Orbitrap mass analyzer). Voltages that ensure high ion transmission (e.g., >80%) are considered optimal here. The SIMION Ion and Electron Optics Simulator (Figure 5) was leveraged to predict optimal lens voltages as a function of target and extractor voltages, initial ion energy, and sample thickness and relative permittivity. In one such model that serves as a case study, a dielectric medium with relative permittivity of 3 was used to simulate the electrical properties of the lunar regolith.[35] Ion generation from the lunar regolith surface was assumed to be Lambertian with ion flux proportional to the cosine of the angle between the emission direction and perpendicular to the surface. Ions from the dielectric surface were assumed to have an intial energy

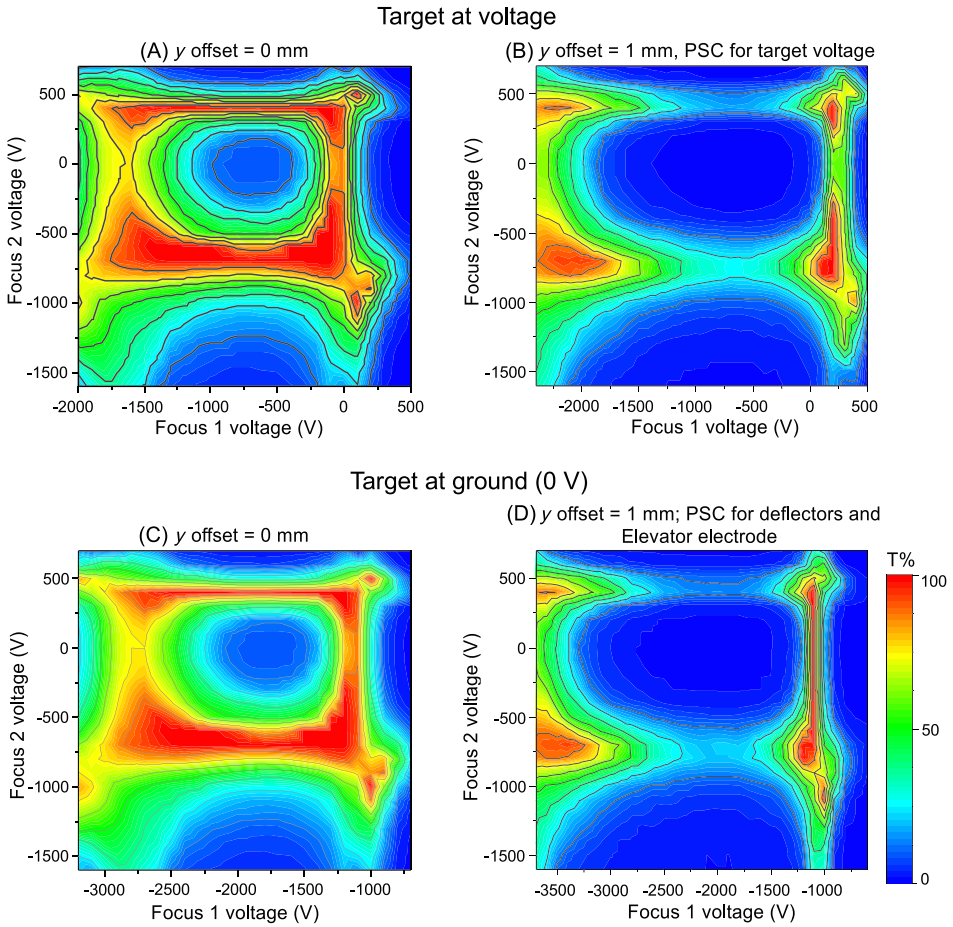

FIGURE 6 Transmission efficiency (T%) of cations (*m*/*z* 133) as a function of focus 1 and focus 2 voltages. These simulations illustrate the influence of sample height from a nominal reference plane (denoted as *y* offset) and the voltage applied to the target. (A) *y* offset = 0 mm, target is held at a nominal voltage of +1100 V, no potential sag compensation (PSC) applied. (B) *y* offset = 1 mm, PSC is applied by holding the target at a higher than nominal voltage, i.e., at +1460 V to compensate for the sag in electrical potential due to sample topography/protrusion through the mechanical stop aperture. (C) *y* offset = 0 mm, target is held at 0 V and elevator electrode is pulsed from −1100 V, no PSC is applied. (D) *y* offset = 1 mm, target is grounded (0 V), PSC is applied by pulsing the deflectors and elevator electrode from −1420 V. The central electrode was ramped exponentially from −3300 V (injection/initial voltage) to −3450 V (final voltage) while the deflector electrode was ramped from 0 V (injection/initial voltage) to +400 V (final voltage). The extractor voltage was set at −1900 V (when target is at voltage, A and B) or −2900 V (when target is at 0 V, C and D). Ramp time constants were 24.2 and 73.5 μs, respectively. The transmission of an ion through the Orbitrap mass analyzer was considered successful when an ion performed three axial oscillations along the CE. [Color figure can be viewed at wileyonlinelibrary.com]

of 1 eV and were accelerated into the ion inlet in a direction parallel to the ion axis. For positive ion simulation, an exponential ramp of the CE and DE within the Orbitrap mass analyzer was initiated 4 μs before ions were generated and tuned to capture ions into nearly circular orbits about the CE. The influence of pressure and space charge was neglected given the short time scale and low laser fluences modeled, respectively. Here, we investigated ion transmission as a function of focus 1 and 2 voltages when varying sample height from the base of the mechanical stop (*y* offset in millimeters) and target voltage, each of which loosely corresponds to modes of sample placement beneath CRATER (Table 2). The dielectric medium simulating lunar regolith was assumed to be flush with the airside (bottom) of the mechanical stop (*y* offset = 0 mm), or extended 1 mm into the mechanical stop (*y* offset = 1 mm), as shown in shown in Figure 5A,B.

The electrostatic potential at the ablation site controls the injection energy of ions generated via laser irradiation. First, when the sample is held at voltage, the open geometry of the aperture within the mechanical stop and position of the dielectric causes the electrostatic potential at the ablation site to shift toward the value of the extractor voltage and results in non-ideal injection energies. When no regolith protrusion is present, i.e., *y* offset = 0 mm (Figure 5A), the potential "sags" only 84 V, which has a negligible effect on ion transmission as illustrated by the wide range of optimal focus 1 and 2 voltages (Figure 6A). However, when the regolith extends 1 mm into the mechanical stop (*y* offset = 1 mm), ion transmission is effectively diminished (not shown here) without the application of a potential sag compensation (PSC). To apply PSC, the voltage applied to the mechanical stop was raised from +1100 V to +1460 V (Figure 6B), enabling ions to be accelerated to energies of 1100 eV and resulting in stable orbits due to better energy matching.[33] The results of these simulations indicate that regolith topography affects ion transmission, and therefore optimization of focus 1 and 2 voltages by application of PSC is essential to ensure efficient ion transmission.

When the sample is grounded, i.e., held at 0 V, the elevator electrode must be pulsed to enable ion injection into the Orbitrap mass analyzer and acquire stable trajectories around the CE. When there is no regolith protrusion into the mechanical stop (*y* offset = 0 mm), ion transmission is high for a broad range of focus voltages (Figure 6C), but a *y* offset of 1 mm (or higher) severely restricts ion transmission even when the elevator electrode is pulsed from −1100 to 0 V. To enable high ion transmission, PSC is applied by floating the deflectors and elevator electrode from −1420 to 0 V (Figure 6D). Simulations of positive ion transmission show that voltages for focus 1 shift to values that are ~1100 V lower (Figure 6C,D) compared to the sample held at voltage (Figure 6A,B), mimicking the shift of the mechanical stop (or target) voltage from 0 to +1100 V. Thus, results obtained with a grounded mechanical stop (i.e., target at 0 V) with a pulsed elevator electrode are similar to those observed for a mechanical stop held at voltage provided the electrostatic potentials of focus 1, extractor, and deflectors are appropriately adjusted.

4 | CRATER PROTOTYPE PERFORMANCE DEMONSTRATION

A prototype of the CRATER instrument, which was assembled at NASA Goddard Space Flight Center in collaboration with the University of Maryland and the French CosmOrbitrap Consortium to empirically optimize operation parameters and demonstrate analytical performance, meets the design and functional specifications of the CRATER protoflight model currently under construction. The prototype instrument includes several commercial power supplies, pulsers, and specialized control circuits to replicate the functionality of the flight electronics system. A central-high speed timing engine based on in-house field programmable gate array code (capable of nanoscond timing accuracy) is triggered by the detected laser pulse. This timing engine handles the synchronization of the time-critical portions of the experiment, i.e., laser pulse energy monitoring and energy control, pulsed voltage application to the elevator electrode, CE, and DE, and transient data collection. The instrument control,

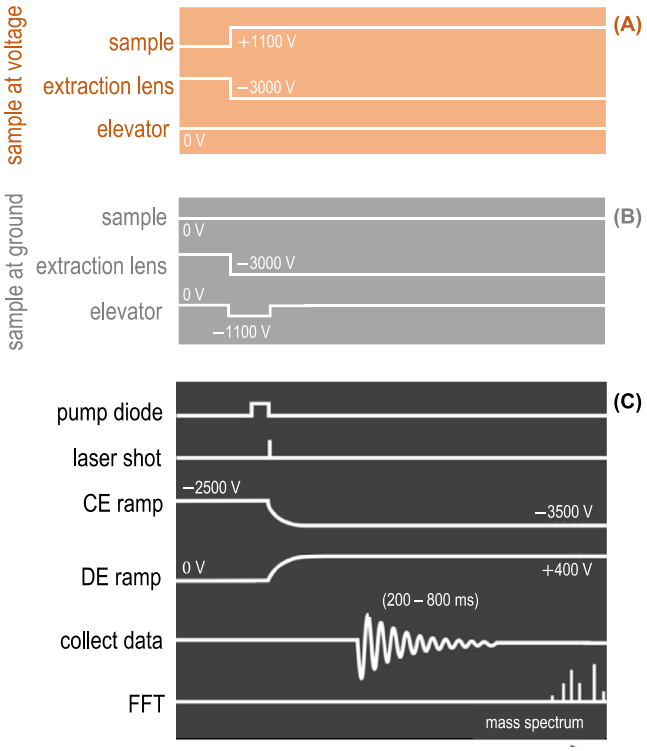

FIGURE 7 Schematic diagram of the analytical sequence of a typical CRATER experiment conducted in positive ion mode, i.e. to detect cations. (A) Voltages when sample is held at voltage and the elevator is at ground. (B) Voltages when sample is held at ground and the elevator is pulsed. (C) Common analytical sequence after (A) or overlapping with (B). The time delay between the central electrode/deflector electrode (CE/DE) voltage ramp and the laser pulse controls the range of *m*/*z* detected. Data acquisition begins after a delay of 1 ms to stabilize the voltage imparted to the CE and to allow enough time for mixed harmonics and side bands associated with radial oscillations to decay.[24] FFT, fast Fourier transform. [Color figure can be viewed at wileyonlinelibrary.com]

synchronization, data collection and processing, as well as health and safety monitoring are accomplished with a National Instruments PXI-based data acquisition system controlled by custom LabVIEW-based software.[36] The CRATER prototype has the capability to analyze samples held at nonzero voltages (Figure 7A) or virtual ground (i.e., 0 V; Figure 7B). The latter mode of operation, which could theoretically support chemical analyses of planetary materials without requiring a complex sample handling system, requires that the elevator electrode be pulsed from −1100 to 0 V (nominally) to "lift" ions to the same electrostatic potential as the Orbitrap analyzer's outer electrodes. This enables the ions to reach the trap with the same kinetic energy they possess in the elevator. When a sample is placed at the laser's focal plane (6 mm from the extractor lens in the baseline design), the laser is fired, the sample ablated and ionized, and the generated ions focused and collimated by the ion inlet and injected into the Orbitrap analyzer. The resulting image current is detected, amplified, and digitized to produce the transient signal.

The lunar crustal surface is characterized by a diverse suite of rocks.[37,38] Basaltic lithologies cover about ~26% of the surface area of the lunar nearside and provide invaluable insights into the deep lunar interior and magma generation processes.[39,40] Samples of lunar basalts have been returned by the Apollo, Luna, and Chang-e missions and have been delivered by meteorites. Although less common, silica-rich lithologies have also been observed on the Moon from remote sensing measurements[41] and felsic clasts discovered in Apollo samples.[42] Here, an example of the instrument's capacity to detect major, minor, and trace elements is demonstrated through the analysis of the USGS standard BIR-1, an Icelandic basalt, and National Institute of Standards and Technology (NIST) Standard Reference Material (SRM) 610, a synthetic silica-rich glass that would fall in the rhyolite field of a traditional total alkali versus silica diagram.

For the analyses, which were conducted under vacuum conditions (<10^{-6} Pa) representative of the ambient lunar surface pressures, BIR-1 powder was pressed onto double-sided conductive carbon tape that was affixed to a sample plate and a solid wafer of NIST SRM 610 was fit into a counterbore in the same plate. Each sample was introduced into the sample chamber via a linear actuator arm and held at a nominal voltage of +1100 V. Data were acquired as 800 ms transients at a sampling rate of 5 MHz. Each such transient was then converted into a frequency spectrum via FFT analysis, followed by conversion into a mass spectrum. Hanning apodization and zero-filling techniques ($2x + n = 2^y$, where x is the length of the original transient, n is the additional transient length required to achieve 2^y, which is the final zero-filled transient length) were applied. Each mass spectrum was then calibrated using the peak for Cs^+ (when present), which is a usual contaminant sourced from the CsI pellet used to monitor the performance of the CRATER instrument, and/or internal calibrants from the sample being analyzed. Each analyte peak of interest was then fit using a Gaussian function to derive peak intensity, centroid, and width at half maximum intensity (Δm). The intensity of each peak reflects the elemental concentration, relative abundance of the observed isotope, and ionization potential of each element in the analyzed sample. The mass accuracy for each measured isotope presented was found within 6 ppm of the true mass. The mass resolving power varied from ~190,000 (at ^{25}Mg) to ~110,000 (at ^{238}U).

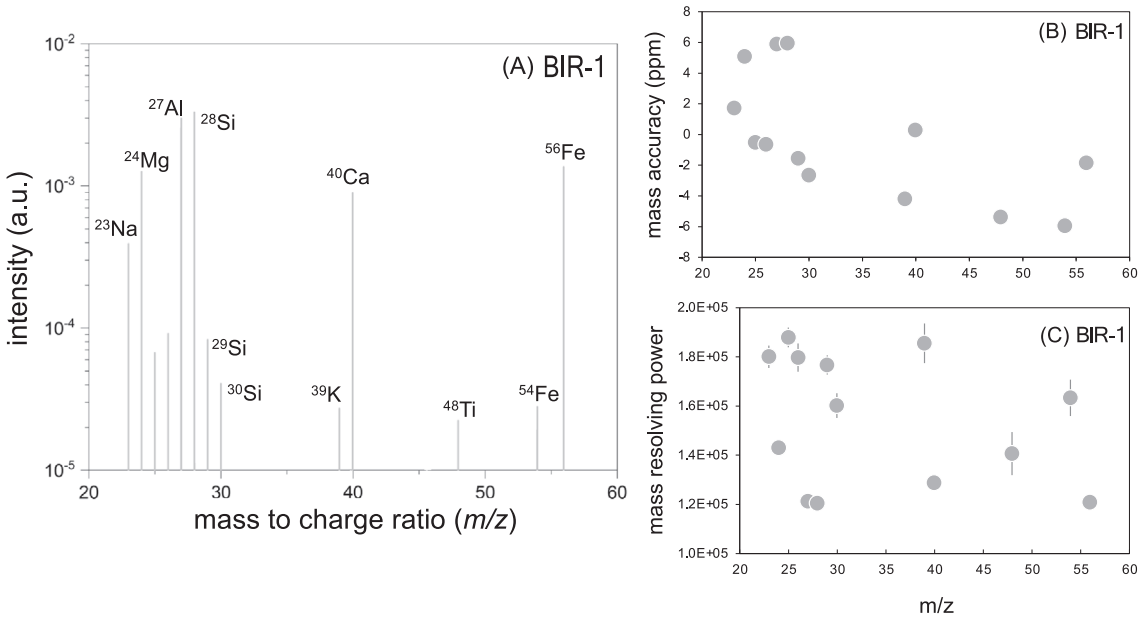

FIGURE 8 (A) Signal intensities of major, minor (Ti 0.575 wt.%), and trace (K 0.025 wt.%) elements in BIR-1 analyzed in positive mode with the CRATER prototype instrument. (B) Mass accuracy (in ppm) vs. m/z. (C) Mass resolving power ($m/\Delta m$ at full width half maximum) vs. m/z of the elements. The BIR-1 mass spectrum was calibrated with $^{28}Si^+$ and $^{56}Fe^+$. Based on its concentration in BIR-1 and signal-to-noise ratio of ~10 observed in this single shot mass spectrum, the detection limit for K (the element with the lowest first ionization potential for the elements shown here) is extrapolated to <100 ppmw.

Lunar mare basalts are typically classified based on their TiO_2 content[39] into very low (<1 wt.%), low (1–6 wt.%), and high Ti (>6 wt.%), reflecting distinct magma source regions and petrogenesis. Potassium and Al have also been utilized to further classify mare basalts.[39] Figure 8A illustrates the detection of Ti, K, Al, and other major elements in BIR-1. Of particular importance to the differentiation of distinct lunar domains are rare earth elements (REE) and Th, which along with other incompatible elements (such as K and P), tend to concentrate in the KREEP component most notably occurring within the Procellarum KREEP Terrane on the lunar nearside.[43] Thorium enrichments have also been characteristic of regions of rare silicic volcanism on the Moon.[41,44] Figure 9A demonstrates CRATER's capabilities to detect trace elements in NIST 610, including diagnostic elements such as the REE and Th critical for inference of lunar petrogenetic processes. All major, minor, and trace elements reported here have been analyzed at better than ±6 ppm mass accuracy (Figures 8B and 9B) and ultrahigh mass resolving power (Figures 8C and 9C). These results validate the projected performance of the CRATER investigation in the context of the prospective lunar mission outlined here (Table 3).

5 | CRATER OPERATIONS DURING A LUNAR MISSION

By providing access to a wide range of geochemical proxies that could inform on outstanding questions in the broader science community (Table 3), such as those prioritized by the NASA Decadal Strategy for Planetary Science and Astrobiology,[45] the Artemis III Science Definition Team Definition Report,[46] and the NASA Science Strategy

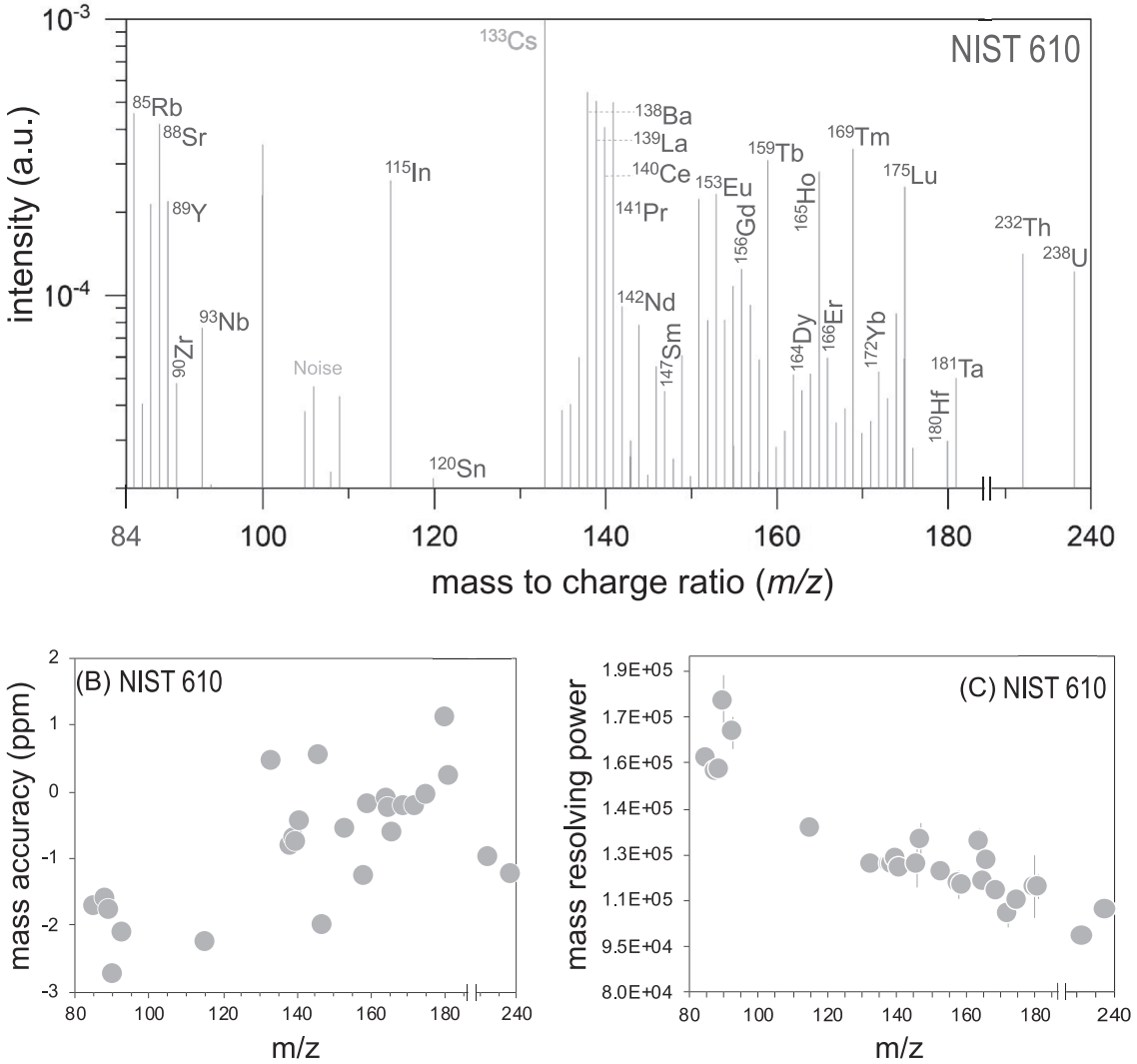

FIGURE 9 (A) Signal intensities of selected trace elements, including rare earth elements (REEs), in NIST 610 analyzed in the positive mode with the CRATER prototype. (B) Mass accuracy (in ppm) vs. m/z. (C) Mass resolving power ($m/\Delta m$ at full width half maximum) vs. m/z of the major elements. The NIST SRM 610 mass spectrum has been calibrated with $^{133}Cs^+$ (external calibrant denoted in light gray text) and a linear term based on internal calibrants $^{85}Rb^+$ and $^{238}U^+$. Based on its concentration in NIST 610 and the signal-to-noise ratio of ~150 determined in this single-shot mass spectrum, the detection limit for Pr (REE with the lowest first ionization potential) is determined to be <5 ppmw.

TABLE 3 Outline of CRATER's role in answering broad science questions during a prospective lunar mission

Broad science goal	CRATER-enabled measurements	Projected performance
Constrain the chemical evolution history of the Moon by analyzing the composition of diverse lunar surface lithologies	Major, minor, and trace element abundances and normative mineralogy Rare earth element (REE) abundances	<1.0 wt.% detection limit for major elements[a] <10 ppm (w/w) detection limit for REE[a]
Characterize the organic inventory of the lunar (sub) surface to assess the delivery, survival, and detectability of exogenous organic materials, and establish a life detection blank for future astrobiology missions	Stoichiometric detection, identification, and classification of refractory organic molecules Abundance patterns of organic compounds and spatial correlations with host mineralogy	pmol/mm^2-level detection limit for amino acids, heterocycles, and aromatic compounds[b] Mass resolving power ($m/\Delta m$) > 100 000 (FWHM at m/z 100)[b] Mass range up to 2000 u[b] Mass accuracy <3 ppm[b]
Assess the resource potential of specific domains on the lunar (sub) surface	Abundance, distribution, and host mineralogy of economic resources	2D chemical imaging with ≤50 μm spatial resolution[c]

Abbreviations: FWHM, full width, half maximum; REE, rare earth element.
[a]Demonstrated during analyses of BIR-1 and NIST 610 standards in this study.
[b]Demonstrated via analyses of organic compounds using breadboard instrument equipped with a 266 nm laser.[20]
[c]Projected based on diffraction limited beam radius for a 213 nm laser.

at the Moon,[47] CRATER could contribute to a host of lunar mission concepts. The CRATER instrument could either be lowered to the lunar surface via a tether or simple translational mechanism (compatible with a mobile rover), or have samples delivered to the mechanical stop of the ion inlet via an articulating robotic arm (compatible with a stationary lander).

In the scenario that CRATER is placed on a mobile lunar rover, sample analyses could be accumulated along a kilometer-scale transect that crosses multiple distinct lithologies; the instrument would only need to be lowered until the mechanical stop makes contact with the surface. In comparison, if CRATER is deployed onboard a spacecraft with limited mobility, a relatively modest robotic arm with only two degrees of freedom (rotation plus one joint) would provide access to multiple samples across the circumference of the arm's extended rotation, expanding the scale of the investigation to the meter scale and maximizing science return. The arm could theoretically dig beneath the uppermost regolith, supporting depth profiling at the landing site. The capacity of LDMS techniques to measure elemental composition (including trace elements down to ppmw levels, as demonstrated here) and characterize the organic inventory of planetary samples (as shown by previous studies[20]) illustrates that CRATER would be a highly valuable addition to any number of CLPS missions. Furthermore, CRATER could complement the payload of missions targeting the South Pole Aitken basin, such as the Endurance-A concept formulated to collect samples for future return by Artemis astronauts.

6 | TECHNICAL RISKS AND MITIGATION STRATEGIES

The primary risks/challenges to the deployment and operation of the CRATER instrument on the lunar surface, or any other planetary destination, include (i) meeting vacuum requirements for maximum analytical performance, (ii) minimizing the risk of particulate accumulation on the extractor electrode (and thus extending operational hours), and (iii) prioritizing data return for mission designs with low bandwidths and/or limited lifetimes. Experiments with the first operational breadboard of CRATER,[25] a path-finding predecessor to the prototype instrument leveraged for this study, identified a decrease in the maximum achievable mass resolving power at pressures above 10^{-6} Pa. Fuel exhaust from the landing event and/or the sublimation of volatiles from the uppermost regolith could incur local pressure rise. Thus, the CRATER design accommodates a vacuum port that could be integrated with an exhaust pipe pointed toward space (i.e., zenith). The end of the exhaust pipe will be sealed with a high-conductance valve, break-off cap, or rupture disc to protect the instrument from contamination (e.g., lofted regolith particles from the landing site and/or hydrazine vapor from the spacecraft descent engines) during descent and landing.

During science operations, lunar regolith will be delivered to the CRATER instrument (or the instrument will be lowered to the lunar surface), potentially lofting fine-grained particles during sample introduction. To minimize the risk of dust accumulation on the CRATER extractor electrode (the optical element nearest the sample surface), the ion inlet is shielded by the mechanical stop, which serves as an effective dust cover. In-house testing has also revealed that applying voltage to the lens stack and rapidly switching polarities can serve as an effective measure to remove dust particles. Nonetheless, dust remains a major challenge for CRATER and other in situ instruments (e.g., cameras) targeting the lunar surface.

Finally, the data volume required to record each mass spectrum is significantly larger than those required by heritage mass analyzers (e.g., SAM onboard the Curiosity rover).[48] Specifically, a single high-resolution mass spectrum (i.e., $m/\Delta m$ > 100,000 FWHM at m/z 100) requires a transient of approximately 839 ms, which translates to a 2^{26} bits (or ~67 Mb) mass spectrum after applying a single zero filling. A 2D chemical map with 50 discrete "pixels" would thus require ~3.4 Gb. Dual-polarity operations would require twice the data volume. Consequently, the application of data compression

techniques and/or progressive machine learning approaches, such as those explored for the MOMA flight instrument,[49] will likely be required to enable more and/or higher value spectra to be returned to Earth on missions with low bandwidths or limited lifetimes.

7 | CONCLUSION

Scientific exploration of the Moon requires the development of spaceflight instruments capable of answering outstanding questions about the formation and evolution of the lunar surface and deep interior. Spaceflight mass spectrometers have continuously expanded their analytical capabilities[50] ever since the first magnetic sector mass analyzers were flown beyond low-Earth orbit as part of the Apollo Program. The CRATER investigation centers on a highly miniaturized LDMS instrument that has been ruggedized for spaceflight and is capable of characterizing the elemental composition (as demonstrated here) and organic inventory of solid samples (as shown previously[20]) with high sensitivity, unparalleled mass resolving power, and ppm-level mass accuracy. Based on a core design that combines the strong suits of both LDMS techniques and the Orbitrap mass analyzer, the CRATER instrument is a frontrunner to usher in the next generation of spaceflight mass spectrometers for the exploration of planetary bodies.

AUTHOR CONTRIBUTIONS

Soumya Ray: Methodology; writing—review and editing; writing—original draft; formal analysis; data curation; investigation. **Ricardo Arévalo:** Funding acquisition; conceptualization; writing—review and editing; writing—original draft. **Adrian Southard:** Writing—original draft; writing—review and editing; methodology; formal analysis. **Lori Willhite:** Writing—review and editing. **Anais Bardyn:** Resources. **Ziqin Ni:** Writing—review and editing. **Ryan Danell:** Writing—original draft; resources; software. **Andrej Grubisic:** Resources. **Cynthia Gundersen:** Writing—review and editing; resources. **Julie Llano:** Writing—review and editing; resources. **Anthony Yu:** Resources; writing—review and editing. **Molly Fahey:** Resources. **Emanuel Hernandez:** Resources. **Jacob Graham:** Resources. **Jane Lee:** Resources; writing—review and editing. **Akif Ersahin:** Resources. **Christelle Briois:** Resources. **Laurent Thirkell:** Resources. **Fabrice Colin:** Resources. **Alexander Makarov:** Writing—review and editing.

PEER REVIEW

The peer review history for this article is available at https://www.webofscience.com/api/gateway/wos/peer-review/10.1002/rcm.9657.

DATA AVAILABILITY STATEMENT

The data that support the findings of this study are available from the corresponding author upon reasonable request.

ORCID

Soumya Ray https://orcid.org/0000-0002-9591-9380
Ricardo Arévalo Jr https://orcid.org/0000-0002-0558-5090
Lori Willhite https://orcid.org/0000-0001-7247-7842
Ziqin Ni https://orcid.org/0000-0003-2616-1630
Ryan Danell https://orcid.org/0000-0003-4863-1998
Christelle Briois https://orcid.org/0000-0002-5616-0180

REFERENCES

1. Lawrence DJ, Feldman WC, Barraclough BL, et al. Global elemental maps of the moon: the lunar prospector gamma-ray spectrometer. *Summarized Proceedings for the Period from and a Directory of Members as of*. 1998;281(5382):1484-1489. doi:10.1126/science.281.5382.1484
2. Ohtake M, Matsunaga T, Haruyama J, et al. The global distribution of pure anorthosite on the moon. *Nature*. 2009;461(7261):236-240. doi:10.1038/nature08317
3. Lucey PG. Mineral maps of the moon. *Geophys Res Lett*. 2004;31(8):3, L08701-6. doi:10.1029/2003GL019406
4. Yamashita N, Hasebe N, Reedy RC, et al. Uranium on the moon: global distribution and U/Th ratio. *Geophys Res Lett*. 2010;37(10). doi:10.1029/2010GL043061
5. Yamashita N, Gasnault O, Forni O, et al. The global distribution of calcium on the moon: implications for high-ca pyroxene in the eastern mare region. *Earth Planet Sci Lett*. 2012;353-354:93-98. doi:10.1016/j.epsl.2012.08.010
6. Yamamoto S, Nakamura R, Matsunaga T, et al. Massive layer of pure anorthosite on the moon. *Geophys Res Lett*. 2012;39(13):1, n/a-6. doi:10.1029/2012GL052098
7. Korotev RL. Lunar geochemistry as told by lunar meteorites. *Chemie der Erde*. 2005;65(4):297-346. doi:10.1016/j.chemer.2005.07.001
8. Warren PH. "New" lunar meteorites: implications for composition of the global lunar surface, lunar crust, and the bulk moon. *Meteorit Planet Sci*. 2005;40(3):477-506. doi:10.1111/j.1945-5100.2005.tb00395.x
9. Wood JA, Dickey JS Jr, Marvin UB, Powell BN. Lunar anorthosites and a geophysical model of the moon. In: *Proceedings of the 11th Lunar Science Conference*. Vol. 1; 1970:965-988.
10. Smith JV, Anderson AT, Newton RC, et al. Petrologic History of the Moon Inferred from Petrography, Mineralogy, and Petrogenesis of Apollo 11 Rocks 1970;1:897-925.
11. Podosek FA, Huneke JC, Gancarz AJ, Wasserburg GJ. The age and petrography of two Luna 20 fragments and inferences for widespread lunar metamorphism. *Geochim Cosmochim Acta*. 1973;37(4):887-904. doi:10.1016/0016-7037(73)90186-5
12. Tian HC, Wang H, Chen Y, et al. Non-KREEP origin for Chang'e-5 basalts in the Procellarum KREEP terrane. *Nature*. 2021;600(7887):59-63. doi:10.1038/s41586-021-04119-5
13. Che X, Nemchin A, Liu D, et al. Age and composition of young basalts on the moon, measured from samples returned by Chang'e-5. *Science*. 2021;374(6569):887-890. doi:10.1126/science.abl7957
14. Vastola FJ, Pirone AJ. *Adv Mass Spectrom*. 1970;4:107.
15. Managadze GG, Wurz P, Sagdeev RZ, et al. Study of the main geochemical characteristics of Phobos' regolith using laser time-of-flight mass spectrometry. *Sol Syst Res*. 2010;44(5):376-384. doi:10.1134/S0038094610050047
16. Goesmann F, Brinckerhoff WB, Raulin F, et al. The Mars organic molecule analyzer (MOMA) instrument: characterization of organic material in Martian sediments. *Astrobiology*. 2017;17(6–7):655-685. doi:10.1089/ast.2016.1551
17. Ligterink NFW, Grimaudo V, Moreno-García P, et al. ORIGIN: a novel and compact laser desorption—mass spectrometry system for sensitive in situ detection of amino acids on extraterrestrial surfaces. *Sci Rep*. 2020;10(1):1, 9641-10. doi:10.1038/s41598-020-66240-1
18. Willhite L, Ni Z, Arevalo R, et al. CORALS: a laser desorption/ablation orbitrap mass spectrometer for in situ exploration of Europa. IEEE

Aerosp Conf Proc. 2021;2021-March:1–13. doi:10.1109/AERO50100.2021.9438221
19. Grubisic A, Trainer MG, Li X, et al. Laser desorption mass spectrometry at Saturn's moon titan. *Int J Mass Spectrom*. 2021;470:116707. doi:10.1016/j.ijms.2021.116707
20. Arevalo R, Willhite L, Bardyn A, et al. Laser desorption mass spectrometry with an Orbitrap analyser for in situ astrobiology. *Nat Astron* Published Online. 2023;7(3):359-365. doi:10.1038/s41550-022-01866-x
21. Jeffries TE, Jackson SE, Longerich HP. Application of a frequency quintupled Nd:YAG source (λ = 213 nm) for laser ablation inductively coupled plasma mass spectrometric analysis of minerals. *J Anal at Spectrom*. 1998;13(9):935-940. doi:10.1039/a801328d
22. Steglich M, Bouwman J, Huisken F, Henning T. Can neutral and ionized polycyclic aromatic hydrocarbons be carriers of the ultraviolet extinction bump and the diffuse interstellar bands? *Astrophys J*. 2011;742(1):2. doi:10.1088/0004-637X/742/1/2
23. Hilchenbach M, Kissel J, Langevin Y, et al. Comet 67P/Churyumov–Gerasimenko: close-up on dust particle fragments. *Astrophys J*. 2016;816(2):L32. doi:10.3847/2041-8205/816/2/l32
24. Makarov A. Electrostatic axially harmonic orbital trapping: a high-performance technique of mass analysis. *Anal Chem*. 2000;72(6):1156-1162. doi:10.1021/ac991131p
25. Briois C, Thissen R, Thirkell L, et al. Orbitrap mass analyser for in situ characterisation of planetary environments: performance evaluation of a laboratory prototype. *Planet Space Sci*. 2016;131:33-45. doi:10.1016/j.pss.2016.06.012
26. Arevalo R, Selliez L, Briois C, et al. An Orbitrap-based laser desorption/ablation mass spectrometer designed for spaceflight. *Rapid Commun Mass Spectrom*. 2018;32(21):1875-1886. doi:10.1002/rcm.8244
27. Selliez L, Briois C, Carrasco N, et al. Identification of organic molecules with a laboratory prototype based on the laser ablation-CosmOrbitrap. *Planet Space Sci*. 2019;170(2018):42-51. doi:10.1016/j.pss.2019.03.003
28. Selliez L, Maillard J, Cherville B, et al. High-resolution mass spectrometry for future space missions: comparative analysis of complex organic matter with LAb-CosmOrbitrap and laser desorption/ionization Fourier transform ion cyclotron resonance. *Rapid Commun Mass Spectrom*. 2020;34(10):e8645. doi:10.1002/rcm.8645
29. Selliez L, Briois C, Carrasco N, et al. Analytical performances of the LAb-CosmOrbitrap mass spectrometer for astrobiology. *Planet Space Sci*. 2022;2023(225):105607. doi:10.1016/j.pss.2022.105607
30. Krebs DJ, Novo-Gradac AM, Li SX, Lindauer SJ, Afzal RS, Yu AW. Compact, passively Q-switched Nd:YAG laser for the MESSENGER mission to mercury. *Appl Optics*. 2005;44(9):1715-1718. doi:10.1364/AO.44.001715
31. Bogaerts A, Chen Z. Effect of laser parameters on laser ablation and laser-induced plasma formation: a numerical modeling investigation. *Spectrochim Acta—Part B at Spectrosc*. 2005;60(9–10):1280-1307. doi:10.1016/j.sab.2005.06.009
32. Fahey M, Yu A, Grubisic A, et al. Ultraviolet Laser Development for Planetary Lander Missions. IEEE Aerosp Conf Proc. Published Online 2020:1-11. doi:10.1109/AERO47225.2020.9172711
33. Hu Q, Noll RJ, Li H, Makarov A, Hardman M, Cooks RG. The Orbitrap: a new mass spectrometer. *J Mass Spectrom*. 2005;40(4):430-443. doi:10.1002/jms.856
34. Perry RH, Cooks RG, Noll RJ. Orbitrap mass spectrometry: instrumentation, ion motion and applications. *Mass Spectrom Rev*. 2008;27(6):661-699. doi:10.1002/mas.20186
35. Zhang L, Zeng Z, Li J, et al. Parameter estimation of lunar regolith from lunar penetrating radar data. *Sensor*. 2018;18(9). doi:10.3390/s18092907
36. Danell, Ryan M. A Full Featured, Flexible, and Inexpensive 2D and 3D Ion Trap Control Architecture and Software Package. Proceedings of the 58th ASMS Conference on Mass Spectrometry and Allied Topics. 2010.
37. Taylor GJ, Warren P, Ryder G, Delano J, Pieters C, Lofgren G. Lunar rocks. In: Heiken GH, Vaniman DT, French BM, eds. *Lunar sourcebook, a user's guide to the moon*. Cambridge University Press; 1991:183-284. ISBN:0521334446.
38. Warren PH, Taylor GJ. The Moon. Vol. 2.; 2013:213-250. doi:10.1016/B978-0-08-095975-7.00124-8
39. Neal CR, Taylor LA. Petrogenesis of mare basalts: a record of lunar volcanism. *Geochim Cosmochim Acta*. 1992;56(6):2177-2211. doi:10.1016/0016-7037(92)90184-K
40. Grove TL, Krawczynski MJ. Lunar mare volcanism: where did the magmas come from? *Elements*. 2009;5(1):29-34. doi:10.2113/gselements.5.1.29
41. Glotch TD, Lucey PG, Bandfield JL, et al. Highly silicic compositions on the moon. *Summarized Proceedings for the Period from and a Directory of Members as of*. 2010;329(5998):1510-1513. doi:10.1126/science.1192148
42. Seddio SM, Jolliff BL, Korotev RL, Zeigler RA. Petrology and geochemistry of lunar granite 12032,366-19 and implications for lunar granite petrogenesis. *Am Mineral*. 2013;98(10):1697-1713. doi:10.2138/am.2013.4330
43. Jolliff BL, Gillis JJ, Haskin LA, Korotev RL, Wieczorek MA. Major lunar crustal terranes: surface expressions and crust-mantle origins. *J Geophys Res Planets*. 2000;105(E2):4197-4216. doi:10.1029/1999JE001103
44. Jolliff BL, Wiseman SA, Lawrence SJ, et al. Non-mare silicic volcanism on the lunar farside at Compton-Belkovich. *Nat Geosci*. 2011;4(8):566-571. doi:10.1038/ngeo1212
45. National Academies of Sciences, Engineering, and Medicine. *Origins, worlds, and life: a decadal strategy for planetary science and astrobiology 2023–2032*. The National Academies Press; 2022. doi:10.17226/26522
46. National Research Council. *The scientific context for exploration of the moon*. The National Academies Press; 2007. doi:10.17226/11954
47. Aeronautics N, Administration S. *Artemis III science definition team report*; 2020.
48. Mahaffy PR, Webster CR, Cabane M, et al. The sample analysis at Mars investigation and instrument suite. *Space Science Reviews*. 2012;170(1-4):401-478. doi:10.1007/s11214-012-9879-z
49. Da Poian V, Lyness E, Danell R, et al. Science autonomy and space science: application to the ExoMars Mission. *FSPAS*. 2022;9(April):1-14. doi:10.3389/fspas.2022.848669
50. Arevalo R, Ni Z, Danell RM. Mass spectrometry and planetary exploration: a brief review and future projection. *J Mass Spectrom*. 2020;55(1):e4454. doi:10.1002/jms.4454

How to cite this article: Ray S, Arévalo R Jr, Southard A, et al. Characterization of Regolith And Trace Economic Resources (CRATER): An Orbitrap-based laser desorption mass spectrometry instrument for in situ exploration of the Moon. *Rapid Commun Mass Spectrom*. 2024;38(6):e9657. doi:10.1002/rcm.9657